Inorg. Chem. **2007**, *46*, 5034–5045

Synthesis and Structural Characterization of $C(OTeF_5)_4$ and a Comparative Structural Study of the Isoelectronic $B(OTeF_5)_4^-$ Anion

Matthew D. Moran, Hélène P. A. Mercier, and Gary J. Schrobilgen*

Department of Chemistry, McMaster University, Hamilton, Ontario, L8S 4M1, Canada

Received February 26, 2007

Tetrakis(pentafluoroorthotellurate)carbon(IV), $C(OTeF_5)_4$, was synthesized by reaction of CBr_4 with $BrOTeF_5$ in SO_2ClF solution at −78 °C and was isolated as a colorless, crystalline solid that is room-temperature stable in SO_2ClF and in the solid state. Both natural abundance and 99% ^{13}C-enriched $C(OTeF_5)_4$ have been characterized in SO_2ClF solution by ^{13}C, ^{19}F, and ^{125}Te NMR spectroscopy. In contrast, $C(OTeF_5)_4$ undergoes rapid decomposition to $O(TeF_5)_2$ and CO_2 in CH_3CN at 10 °C but is stable at −40 °C. The X-ray crystal structures of $C(OTeF_5)_4$ and $[N(CH_3)_4][B(OTeF_5)_4]$ were determined at −30 and −170 °C, respectively. The averages of four smaller C/B–O–Te bond angles and O···O contacts and two larger C/B–O–Te bond angles and O···O contacts of $C(OTeF_5)_4$ and the isoelectronic $B(OTeF_5)_4^-$ anion are consistent with local S_4 symmetry, as predicted by ligand close packing considerations. The existence of three sets of Te–O–C/B–O torsion angles and the energy-minimized geometries of $C(OTeF_5)_4$ and $B(OTeF_5)_4^-$ also confirm their local S_4 symmetries. The low-temperature, solid-state Raman spectra of $^{12/13}C(OTeF_5)_4$ and $B(OTeF_5)_4^-$ were assigned and compared. The energy-minimized geometries, vibrational frequencies, natural charges, and natural bond orders of both species have been calculated using density functional theory methods. The calculated geometries are in accord with the S_4 symmetries assigned for the experimental structures.

Introduction

Although organic examples of orthocarbonates ($C(OR)_4$) abound,[1,2] very few C−O bonded tetrakis-compounds containing inorganic ligands are known, namely, $C(OSO_2F)_4$,[3] $C(OCF_3)_4$,[4,5] and $C(OSeF_5)_4$.[6] Although the chemistries of the $OSeF_5$ and $OTeF_5$ ligands are similar, no detailed study of the $OTeF_5$ analogue, $C(OTeF_5)_4$, has appeared in the literature. Prior to this study, the only fully $OTeF_5$-substituted derivatives of the row 2 elements that have been structurally characterized are $B(OTeF_5)_3$,[7,8] $B(OTeF_5)_4^-$,[9−11] $O(TeF_5)_2$,[12−14] $(OTeF_5)_2$,[15,16] and $FOTeF_5$.[17,18] The complete $CH_n(OSeF_5)_{4-n}$ ($n = 0-3$) series has been synthesized by reaction of the corresponding chlorohydrocarbon with $Hg(OSeF_5)_2$ in n-C_6F_{14} and characterized by infrared and Raman spectroscopy, NMR spectroscopy, and mass spectrometry.[6] No crystal structure is available for $C(OSeF_5)_4$, but unit cell parameters have been reported.[6] Although several monosubstituted alkyl $OTeF_5$ derivatives, $ROTeF_5$, have been prepared by reaction of TeF_6 with ROH (R = Me, Et, Pr, $CHMe_2$, Bu, CHMeEt,

* To whom correspondence should be addressed. E-mail: schrobil@mcmaster.ca.

(1) Diaper, C. M. *Sci. Synth.* **2005**, *18*, 1203−1282.
(2) Lebel, H.; Grenon, M. *Sci. Synth.* **2005**, *22*, 669−747.
(3) DesMarteau, D. D. *Inorg. Chem.* **1968**, *7*, 434−437.
(4) Adcock, J. L.; Robin, M. L.; Zuberi, S. *J. Fluorine Chem.* **1987**, *37*, 327−336.
(5) Lin, W. H.; Clark, W. D.; Lagow, R. J. *J. Org. Chem.* **1989**, *54*, 1990−1992.
(6) Huppmann, P.; Lentz, D.; Seppelt, K. *Z. Anorg. Allg. Chem.* **1981**, *472*, 26−32.
(7) Kropshofer, H.; Leitzke, O.; Peringer, P.; Sladky, F. O. *Chem. Ber.* **1981**, *114*, 2644−2648.
(8) Sawyer, J. F.; Schrobilgen, G. J. *Acta Crystallogr.* **1982**, *B38*, 1561−1563.
(9) Noirot, M. D.; Anderson, O. P.; Strauss, S. H. *Inorg. Chem.* **1987**, *26*, 2216−2223.
(10) Hurlburt, P. K.; Anderson, O. P.; Strauss, S. H. *J. Am. Chem. Soc.* **1991**, *113*, 6277−6278.
(11) Hurlburt, P. K.; Anderson, O. P.; Strauss, S. H. *Can. J. Chem.* **1992**, *70*, 726−731.
(12) Engelbrecht, A.; Loreck, W.; Nehoda, W. *Z. Anorg. Allg. Chem.* **1968**, *360*, 88−96.
(13) Buerger, H. *Z. Anorg. Allg. Chem.* **1968**, *360*, 97−103.
(14) Oberhammer, H.; Seppelt, K. *Angew. Chem., Int. Ed. Engl.* **1978**, *17*, 69−70.
(15) Seppelt, K.; Nothe, D. *Inorg. Chem.* **1973**, *12*, 2727−2730.
(16) Zylka, P.; Oberhammer, H.; Seppelt, K. *J. Mol. Struct.* **1991**, *243*, 411−418.
(17) Schack, C. J.; Wilson, W. W.; Christe, K. O. *Inorg. Chem.* **1983**, *22*, 18−21.
(18) Schack, C. J.; Christe, K. O. *Inorg. Chem.* **1984**, *23*, 2922.

10.1021/ic700362g CCC: $37.00
Published on Web 05/16/2007

CH_2CHMe_2),[19] the isolation and full structural characterization of $C(OTeF_5)_4$ have not been reported.

More recently, $C(OTeF_5)_4$ has been generated and characterized in SO_2ClF solution by ^{13}C and ^{19}F NMR spectroscopy for comparison with the NMR parameters of the $C(OTeF_5)_3^+$ cation.[20] The present Article provides the detailed synthesis, solution multi-NMR and solid-state characterizations of $C(OTeF_5)_4$ by X-ray crystallography and Raman spectroscopy, and a study of its decomposition in CH_3CN. The $[N(CH_3)_4][B(OTeF_5)_4]$ salt has been synthesized, and its crystal structure and Raman spectrum have been acquired for comparison of the geometrical parameters of $B(OTeF_5)_4^-$ with those of isoelectronic $C(OTeF_5)_4$. Electronic structure calculations for both the $C(OTeF_5)_4$ and the $B(OTeF_5)_4^-$ anion were carried out using density functional theory (DFT) methods to obtain the energy-minimized gas-phase structures for comparison with their solid-state geometries and to assist in the assignments of their Raman spectra.

Results and Discussion

Synthesis of C(OTeF$_5$)$_4$ and Solution Characterization by ^{13}C, ^{19}F, and ^{125}Te NMR Spectroscopy. The reaction of stoichiometric amounts of $BrOTeF_5$ and CBr_4 in SO_2ClF solution gave nearly quantitative yields of $C(OTeF_5)_4$ with the elimination of Br_2 according to eq 1. Solvent and Br_2 were removed under dynamic vacuum between −78 and 0 °C, yielding colorless, microcrystalline $C(OTeF_5)_4$ which

$$CBr_4 + 4\,BrOTeF_5 \rightarrow C(OTeF_5)_4 + 4\,Br_2 \qquad (1)$$

is stable indefinitely at room temperature.

The full solution NMR characterization of $C(OTeF_5)_4$ in SO_2ClF solution at 30 °C by ^{13}C, ^{19}F, and ^{125}Te NMR spectroscopy relies upon 99% ^{13}C-enrichment and, in particular, on the ^{13}C NMR spectrum of $^{13}C(OTeF_5)_4$ (Figure 1a). The ^{13}C resonance of $C(OTeF_5)_4$ is a singlet at 115.6 ppm that is accompanied by ^{123}Te ($^2J(^{13}C-^{123}Te)$, 54.7 Hz) and ^{125}Te ($^2J(^{13}C-^{125}Te)$, 64.5 Hz) satellites. The ^{13}C environment is significantly more shielded relative to that of the $C(OTeF_5)_3^+$ cation (168.8 ppm).[20] Separate integrations of ^{123}Te (0.87% natural abundance) and ^{125}Te (6.99% natural abundance) satellites were not possible as a result of peak overlap ($\Delta\nu_{1/2} \approx 3$ Hz); thus, the weaker ^{123}Te satellites are not fully resolved and appear as shoulders on the ^{125}Te satellites. Because ^{123}Te and ^{125}Te are spin-$^1/_2$ nuclei of low abundance, only a superposition of subspectra arising from the most abundant isotopomers, $^{13}C(O^0TeF_5)_4$ (singlet), $^{13}C(O^{123/125}TeF_5)(O^0TeF_5)_3$ (doublet), and $^{13}C(O^{125}TeF_5)_2(O^0TeF_5)_2$ (triplet), where ^0Te represents all spinless isotopes of tellurium, was observed. Taking into account the natural isotopic abundances, multiplicities, and statistical distributions of tellurium isotopomers[21] among the

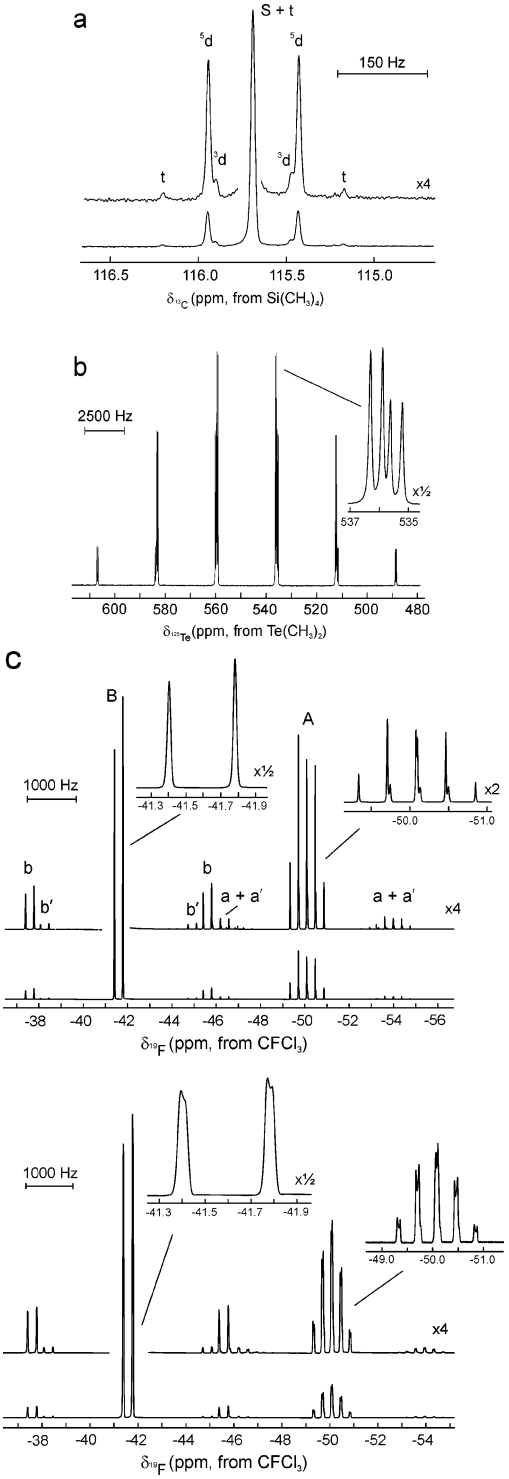

Figure 1. The NMR spectra of $C(OTeF_5)_4$ recorded in SO_2ClF solution at 30 °C: (a) the ^{13}C NMR spectrum (150.903 MHz) of 99% ^{13}C-enriched $C(OTeF_5)_4$. Natural abundance tellurium isotopomer contributions correspond to S (singlet, $^{13}C(O^0TeF_5)_4$, where ^0Te signifies all spinless tellurium isotopes), and satellites are denoted by $^{3/5}$d (doublet, $^{13}C(O^{123/125}TeF_5)(O^0TeF_5)_3$) and t (triplet, $C(O^{125}TeF_5)_2(O^0TeF_5)_2$). (b) The ^{125}Te NMR (157.869 MHz) spectrum of 99% ^{13}C-enriched $C(OTeF_5)_4$. The inset is an expansion of the four most intense lines of the doublet of quintets. (c) The ^{19}F NMR spectra (470.592 MHz) of natural abundance $C(OTeF_5)_4$ (top trace) and 99% ^{13}C-enriched $C(OTeF_5)_4$ (bottom trace). The equatorial and axial fluorine environments of the AB_4 spin systems are denoted by B and A, respectively. Tellurium satellites are denoted by lower case letters, i.e., a and b (^{125}Te) and a′ and b′ (^{123}Te).

(19) Fraser, G. W.; Millar, J. B. *J. Chem. Soc., Dalton Trans.* **1974**, 2029−2031.
(20) Mercier, H. P. A.; Moran, M. D.; Schrobilgen, G. J.; Steinberg, C.; Suontamo, R. J. *J. Am. Chem. Soc.* **2004**, *126*, 5533−5548.
(21) Björgvinsson, M.; Sawyer, J. F.; Schrobilgen, G. J. *Inorg. Chem.* **1987**, *26*, 741−749.

Table 1. Crystallographic Data for $C(OTeF_5)_4$ and $B(OTeF_5)_4^-$

chem formula	$CO_4F_{20}Te_4$	$H_{12}BC_4NO_4F_{20}Te_4$
space group	*Pc* (No. 7)	C_2 (No. 5)
a (Å)	9.9176(4)	17.9521(10)
b (Å)	17.9965(6)	7.7195(1)
c (Å)	20.9666(8)	16.6623(10)
β (deg)	92.445(2)	94.963(2)
V (Å^3)	3738.8(3)	2300.4(4)
molecules/unit cell	8	4
mol wt (g mol^{-1})	966.38	1039.32
calcd density (g cm^{-3})	3.434	3.001
T (°C)	−30	−170
μ (mm^{-1})	7.18	5.20
R_1[a]	0.0530	0.0259
wR_2[b]	0.0944	0.0419

[a] R_1 is defined as $\sum||F_o| - |F_c||/\sum|F_o|$ for $I > 2\sigma(I)$. [b] wR_2 is defined as $[\sum[w(F_o^2 - F_c^2)^2]/\sum w(F_o^2)^2]^{1/2}$ for $I > 2\sigma(I)$.

four sites, the experimental combined $^{123/125}$Te integrated satellite peak/central peak area ratios (0.0116:0.1696:1.0000:0.1687:0.0126) in the ^{13}C NMR spectrum confirm the presence of four equivalent tellurium atoms when compared with their calculated relative intensity ratios (3×10^{-6}:0.0003:0.0107:0.1678:1.0000:0.1678:0.0107:0.0003:3×10^{-6}).

The ^{125}Te NMR spectrum of 99% ^{13}C-enriched $C(OTeF_5)_4$ (Figure 1b) consists of a well-resolved binomial doublet of doublets of quintets ($\delta(^{125}Te)$, 547.6 ppm) arising from $^2J(^{125}Te-^{13}C) = 65.8$ Hz, $^1J(^{125}Te-^{19}F_A) = 3650$ Hz, and $^1J(^{125}Te-^{19}F_B) = 3756$ Hz. The ^{125}Te chemical shift is in good agreement with published values of other $OTeF_5$ compounds.[22−25]

The ^{19}F NMR spectrum of the natural abundance $C(OTeF_5)_4$ (Figure 1c) consists of an AB_4 pattern with accompanying ^{123}Te and ^{125}Te satellites and agrees well with previously reported parameters.[20] The NMR spectrum of 99% ^{13}C-enriched $C(OTeF_5)_4$ ($\delta(^{19}F_B)$, −41.6 ppm; $\delta(^{19}F_A)$, −50.1 ppm; $^2J(^{19}F_A-^{19}F_B)$, 180 Hz; Figure 1c) shows further splitting of the A part of the spectrum arising from $^3J(^{19}F_A-^{13}C) = 24.5$ Hz and of the B_4 part arising from $^3J(^{19}F_B-^{13}C) = 12.1$ Hz.

The behavior of $C(OTeF_5)_4$ in CH_3CN is in marked contrast with its behavior in the less basic solvent, SO_2ClF, where it is stable indefinitely at 30 °C. In an attempt to obtain a long-acquisition-time ^{13}C NMR spectrum of ^{13}C-enriched $C(OTeF_5)_4$ in CH_3CN at 30 °C, only CO_2 was observed. A study of the decomposition of $C(OTeF_5)_4$ in CH_3CN at −40 °C by ^{13}C and ^{19}F NMR spectroscopy revealed that during dissolution at 10 °C, followed by immediate quenching of the reaction at −40 °C and recording the NMR spectra at this temperature, $C(OTeF_5)_4$ reacts to form $O(TeF_5)_2$ and CO_2 (Scheme 1). The NMR parameters of $O(TeF_5)_2$ ($\delta(^{19}F_A)$, −47.0 ppm; $\delta(^{19}F_B)$, −37.1 ppm; $^2J(^{19}F_A-^{19}F_B) = 182$ Hz)[26] and CO_2 ($\delta(^{13}C)$, 126.0 ppm)[27] were in good agreement with the previously reported values. The proposed decomposition pathway is supported by tentative evidence for the reactive intermediate, $O{=}C(OTeF_5)_2$ (mol % composition: 4.2% $O{=}C(OTeF_5)_2$, 49.5% $C(OTeF_5)_4$, and 46.3% $O(TeF_5)_2$). Only the B_4 part of the spectrum of $O{=}C(OTeF_5)_2$ was observed ($\delta(^{19}F_B)$, −40.0 ppm), whereas the A part of the spectrum was obscured by the A parts of the more intense $C(OTeF_5)_4$ and $O(TeF_5)_2$ spectra. Further warming resulted in complete conversion of $C(OTeF_5)_4$ to $O(TeF_5)_2$ and CO_2. The decomposition of $O{=}C(OTeF_5)_2$ to CO_2 and $O(TeF_5)_2$ is supported by the analogous decomposition pathway established for $C(OSO_2F)_4$ which gives rise to CO_2 and $S_2O_5F_2$.[28] Under natural abundance conditions, the ^{13}C NMR spectrum of $O{=}C(OTeF_5)_2$ could not be observed presumably because of its low concentration and the long relaxation time associated with a fully oxygen-substituted carbon species.

The proposed decomposition pathway for $C(OTeF_5)_4$ has features in common with the reaction of CH_3CN with $Nb(OTeF_5)_6^-$ which yields $NbO(OTeF_5)_4(NCCH_3)^-$ and has been observed by ^{19}F NMR spectroscopy.[29] Both reactions lead to intramolecular elimination of $O(TeF_5)_2$ and are apparently initiated by nitrogen coordination of CH_3CN. In the latter case, the seven-coordinate complex anion intermediate, $Nb(OTeF_5)_6(CH_3CN)^-$, is presumably formed, whereas the reaction of $C(OTeF_5)_4$ is unlikely to proceed by S_N2 attack of CH_3CN at the carbon atom of $C(OTeF_5)_4$. Rather, solvent coordination to the tellurium atom of an $OTeF_5$ ligand may occur, which results in expansion of the tellurium valence shell to seven, followed by intramolecular $O(TeF_5)_2$ elimination and $O{=}C(OTeF_5)_2$ formation. Nucleophilic attack of tellurium by CH_3CN may be facilitated by solvent complexation with one or more fluorines of the $OTeF_5$ group, which would build up a positive charge on tellurium, thus activating it for attack by CH_3CN.

Differential Scanning Calorimetry (DSC). During the course of the X-ray crystal structure determination of $C(OTeF_5)_4$, it was found that crystals grown at room temperature by sublimation quickly powdered when handled at or below −100 °C. The phase transition temperature, determined by DSC, showed that an exothermic transition took place at −51.2 °C, releasing 5.73 kJ mol^{-1} of energy. Consequently, X-ray data were collected at −30 °C, which is well above the phase transition temperature. An endothermic phase transition, corresponding to the melting point, occurred at 33.6 °C (heat of fusion, 9.70 kJ mol^{-1}). A second cycle was performed but showed no transitions, consistent with decomposition and/or reaction with the aluminum sample container between the melting point and 125 °C.

X-ray Crystal Structures of $C(OTeF_5)_4$ and $[N(CH_3)_4][B(OTeF_5)_4]$. Details of data collection parameters and other crystallographic information are provided in

(22) Mercier, H. P. A.; Sanders, J. C. P.; Schrobilgen, G. J. *J. Am. Chem. Soc.* **1994**, *116*, 2921−2937.
(23) Mercier, H. P. A.; Sanders, J. C. P.; Schrobilgen, G. J. *Inorg. Chem.* **1995**, *34*, 5261−5273.
(24) Casteel, W. J., Jr.; MacLeod, D. M.; Mercier, H. P. A.; Schrobilgen, G. J. *Inorg. Chem.* **1996**, *35*, 7279−7288.
(25) Mercier, H. P. A.; Moran, M. D.; Sanders, J. C. P.; Schrobilgen, G. J.; Suontamo, R. J. *Inorg. Chem.* **2005**, *44*, 49−60.
(26) Sanders, J. C. P.; Schrobilgen, G. J. *J. Chem. Soc., Chem. Commun.* **1989**, 1576−1578.
(27) Ettinger, R.; Blume, P.; Patterson, A.; Lauterbur, P. C. *J. Magn. Reson.* **1972**, *33*, 1597−1598.
(28) Lustig, M. *Inorg. Chem.* **1965**, *4*, 1828−1830.
(29) Van Seggen, D. M.; Hurlburt, P. K.; Anderson, O. P.; Strauss, S. H. *Inorg. Chem.* **1995**, *34*, 3453−3464.

Table 2. Experimental[a] and Calculated[b] Geometrical Parameters for $C(OTeF_5)_4$ and $B(OTeF_5)_4^-$

	$C(OTeF_5)_4$		
	exptl (C_1) [av]	calcd (C_1)	calcd (S_4)
	ΔE (kJ mol^{-1})		
	0.00 C(4) −39.99 C(2) −92.27 C(1)	−173.42	−173.32
	Bond Lengths (Å)		
C−O	1.35(2)−1.42(2) [1.38(3)]	1.376−1.377 [1.377]	1.376
O−Te	1.85(1)−1.92(1) [1.89(2)]	1.925−1.925 [1.925]	1.925
Te−F	1.74(1)−1.88(1) [1.80(3)]	1.840−1.850 [1.844]	1.839−1.850
	Bond Angles (deg)		
O−C−O (×2)[d]	110(2)−116(1) [113(2)]	112.9, 113.0 [113.0]	113.0
O−C−O (×4)[d]	105(1)−111(1) [108(2)]	107.7−107.8 [107.8]	107.8
C−O−Te	127(1)−131(1) [129(1)]	123.8−123.8 [123.8]	123.7
O−Te−F_a	170.8(7)−177.7(6) [175(2)]	176.4−178.7 [177.6]	176.1
O−Te−F_e	83.9(7)−96.7(7) [90(4)]	85.8−93.7 [90.1]	85.8−93.7
	Torsion Angle (deg)[e]		
	155(1)−174(1) [168(5)]	169.3−169.7 [169.5]	169.3
Te−O−C−O (×4)	29(3)−55(2) [46(7)]	47.2−47.5 [47.4]	47.0
	63(2)−87(2) [73(7)]	71.4−71.7 [71.6]	71.9
	O···O (Å)[d,f]		
aa (×2)	2.28(2)−2.33(2) [2.31(3)]	2.294, 2.296 [2.295]	2.294
ac (×4)	2.16(2)−2.27(2) [2.23(3)]	2.223−2.224 [2.224]	2.224

	$B(OTeF_5)_4^-$			
	exptl (C_1) [av]	calcd (C_1)	calcd (S_4) (one imaginary frequency)[c]	calcd (S_4)
		ΔE (kJ mol^{-1})		
	0.00	−28.99	−31.31	−31.13
		Bond Lengths (Å)		
B−O	1.463(5)−1.476(5) [1.471(6)]	1.455−1.457 [1.456]	1.456	1.457
O−Te	1.828(2)−1.834(2) [1.831(3)]	1.857−1.858 [1.858]	1.857	1.855
Te−F	1.821(3)−1.844(2) [1.830(6)]	1.854−1.861 [1.857]	1.855−1.860	1.854−1.860
		Bond Angles (deg)		
O−B−O (×2)[d]	113.7(3), 113.8(3) [113.8(7)]	113.3, 115.0 [114.2]	111.5	109.5
O−B−O (×4)[d]	106.8(3)−107.9(3) [107.4(5)]	106.6−107.7 [107.2]	108.4	109.4
B−O−Te	128.2(2)−131.6(2) [130(2)]	124.9−128.8 [126.9]	126.2	127.8
O−Te−F_a	173.6(1)−177.1(1) [176(2)]	176.7−178.8 [177.9]	176.4	176.3
O−Te−F_e	89.0(1)−96.0(1) [93(2)]	89.4−96.2 [93.0]	89.7−95.7	90.0−95.9
		Torsion Angle (deg)[e]		
	170.4(2)−179.7(2) [174(4)]	173.7−179.4 [176.6]	151.2	135.3
Te−O−B−O (×4)	47.3(4)−57.9(4) [52(5)]	49.7−58.7 [54.2]	29.9	15.2
	61.1(4)−71.3(4) [67(5)]	60.0−68.6 [64.3]	89.4	104.8
		O···O (Å)[d,f]		
aa (×2)	2.460(4), 2.470(4) [2.465(8)]	1.435, 2.454 [2.445]	2.408	2.386
ac (×4)	2.366(4)−2.376(4) [2.371(5)]	2.335−2.352 [2.344]	2.363	2.378

[a] The quoted geometrical parameters are for the nondisordered $C(OTeF_5)_4$ molecules. [b] SVWN/(SDB-)cc-pVTZ. [c] The geometrical parameters correspond to the S_4 geometry having the lowest energy. [d] Distinctions between the two sets of O−C−O angles and O···O contacts were initially made for each molecule. The values given correspond to the ranges of each set of angles/contacts. [e] The full list of Te−O−C/B−O torsion angles is given in Table S1. [f] The symbols *ac* and *aa* refer to the O···O contact distances for $A(OX)_4$-type molecules of S_4 symmetry as defined in ref 33.

Scheme 1. Proposed Reaction Pathway for the Decomposition of $C(OTeF_5)_4$ in CH_3CN at 10 °C

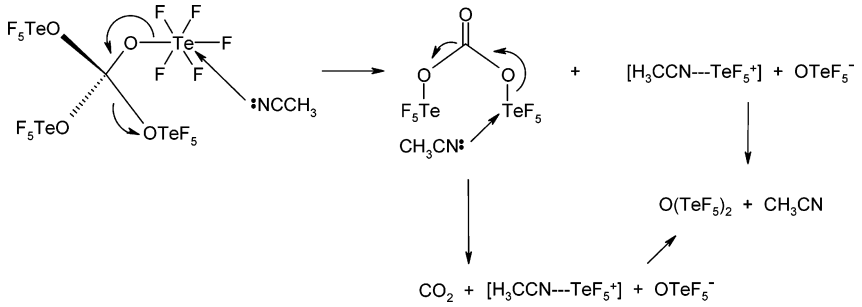

Table 1. Bond lengths, bond angles, torsion angles, and O···O contact distances are listed in Table 2. In order to compare the symmetries for $E(OTeF_5)_4^{-/0}$ (E = B, C), the geometric parameters of the $B(OTeF_5)_4^-$ anion were determined for $[N(CH_3)_4][B(OTeF_5)_4]$ with the view to obtain a structure in which the cation-anion interactions would be

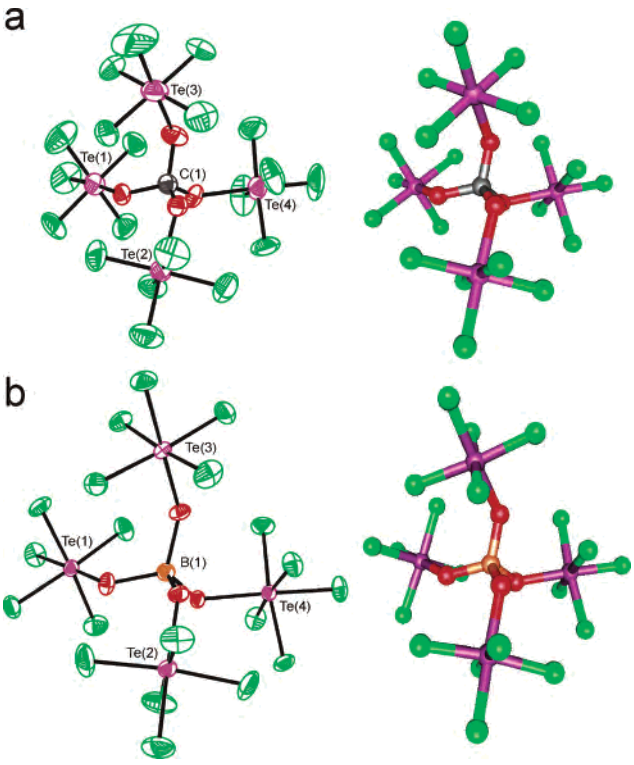

Figure 2. X-ray crystal structures of $C(OTeF_5)_4$ and $B(OTeF_5)_4^-$, where thermal ellipsoids are shown at the 50% probability level: (a) a view of an ordered $C(OTeF_5)_4$ molecule (left) and the calculated geometry of the $C(OTeF_5)_4$ molecule (right); (b) a view of the $B(OTeF_5)_4^-$ anion (left) and the calculated geometry of the $B(OTeF_5)_4^-$ anion (right).

minimized so that the anion closely approximates the calculated gas-phase geometry (see Computational Results).

The symmetries of $C(OTeF_5)_4$ and $B(OTeF_5)_4^-$ are not constrained by the crystal symmetries, with all atoms on general positions. The unit cell of $C(OTeF_5)_4$ contains eight molecules that are generated from four crystallographically independent molecules which all occupy C_1 sites. Three of the crystallographically independent molecules are ordered, and the remaining molecule is affected by a 60:40 positional disorder (see Solutions and Refinements of the Structures and Figure S1 in Supporting Information). Only the geometric parameters of the three unique, ordered molecules are considered in the ensuing discussion. There are 11 F···F contacts near or below the sum of the van der Waals radii (2.94 Å)[30] in $C(OTeF_5)_4$. These range from 2.81(2) to 2.99(2) Å and are in accord with well-isolated molecules. The structure of $[N(CH_3)_4][B(OTeF_5)_4]$ is well-ordered. The $B(OTeF_5)_4^-$ anion has seven unique long H···F contacts, ranging from 2.47 to 2.65 Å, that are at or near the sum of the hydrogen and fluorine van der Waals radii (2.67 Å),[30] consistent with a well-isolated anion.

(a) Bond Lengths and Bond Angles. The $C(OTeF_5)_4$ molecule (Figure 2a) possesses C−O bond lengths (1.35(2)−1.42(2) Å) that are, on average, longer than those reported for the $C(OTeF_5)_3^+$ cation (1.258(15)−1.313(16) Å)[20] and in accord with the expectation that the C−O bonds of the cation will be more covalent. In contrast, the average C−O bond lengths of $C(OTeF_5)_4$ are shorter than those of the isoelectronic $B(OTeF_5)_4^-$ anion (Figure 2b, 1.465(5)−1.476(5) Å), which, because of its formal negative charge, is expected to possess B−O bonds that are more polar than the C−O bonds of its carbon analogue. The decrease in E−O (E = B, C) bond lengths upon increasing the net positive charge is paralleled by an increase in the Te−O bond lengths ($B(OTeF_5)_3$, 1.874(6) Å; $C(OTeF_5)_3^+$, 1.974(8)−1.988(7) Å; $B(OTeF_5)_4^-$, 1.828(2)−1.835(3); $C(OTeF_5)_4$, 1.85(1)−1.92(1) Å). These trends are reproduced by the calculated geometries and NBO analyses (see Computational Results). The Te−F (1.74(1)−1.88(1) Å) bond lengths are in good agreement with those of $B(OTeF_5)_4^-$ (1.819(3)−1.841(2) Å) and those of previously determined $B(OTeF_5)_4^-$ structures.[9−11,31,32]

(b) Molecular Symmetries. (i) Background. Ligand close packing (LCP) considerations have shown that $A(OX)_4$ systems possess either S_4 or D_{2d} symmetries, depending on the effective radii of the oxygen ligand atoms.[33] Because the A−O−X angles are bent, the LCP approach for this class of molecules is based upon an electron density distribution around the oxygen that is not axially symmetric, with the oxygen atom having different ligand radii in different directions. These radii are denoted as *c*, the ligand radius opposite the O−X bond, and *a*, the two ligand radii on either side of the O−X bond, and represent the interligand O···O contact distances which can be associated with D_{2d} or S_4 symmetry.[33] With the use of LCP criteria, an $A(OX)_4$ molecule having S_4 symmetry will have two *a*···*a* and four *a*···*c* interligand contact distances (hereafter denoted as *aa* and *ac*, where *aa* > *ac*[33]), which is differentiated from D_{2d} symmetry which has four *aa* and two *cc* contact distances. Although the ligand-ligand contact distances are reflected in the O−A−O angles, the latter distances are not explicitly discussed.[33]

Previously reported structures of well-isolated $B(OTeF_5)_4^-$ anions[9,11,31,32] have been described as having approximate S_4 symmetry.[31] It was noted that for $B(OTeF_5)_4^-$ to possess rigorous local S_4 symmetry (the fluorine atoms were ignored as they are in the present discussion), one set of four Te−O−B−O torsion angles must be 180°, while the other two sets of four torsion angles must be equal in magnitude but opposite in sign.[31] In fact, these criteria apply to a structure possessing local D_{2d} symmetry. Electronic structure calculations in the present work show that the energy-minimized geometries of $E(OTeF_5)_4^{0/-}$ (E = C, B) possess S_4 symmetry without meeting these criteria (see Computational Results).

(ii) Experimental Geometries. In the present study, the O−B−O bond angles of $B(OTeF_5)_4^-$ (Table 2) possess precisions sufficient to differentiate tetrahedral from non-tetrahedral angles. The average angles were 113.8(7)° for two angles and 107.4(5)° for four angles. In the case of

(30) Bondi, A. *J. Phys. Chem.* **1964**, *68*, 441−451.
(31) Van Seggen, D. M.; Hurlburt, P. K.; Noirot, M. D.; Strauss, S. H. *Inorg. Chem.* **1992**, *31*, 1423−1430.
(32) Hurlburt, P. K.; Rack, J. J.; Luck, J. S.; Dec, S. F.; Webb, J. D.; Anderson, O. P.; Strauss, S. H. *J. Am. Chem. Soc.* **1994**, *116*, 10003−10014.
(33) Heard, G. L.; Gillespie, R. J.; Rankin, D. W. H. *J. Mol. Struct.* **2000**, *520*, 237−248.

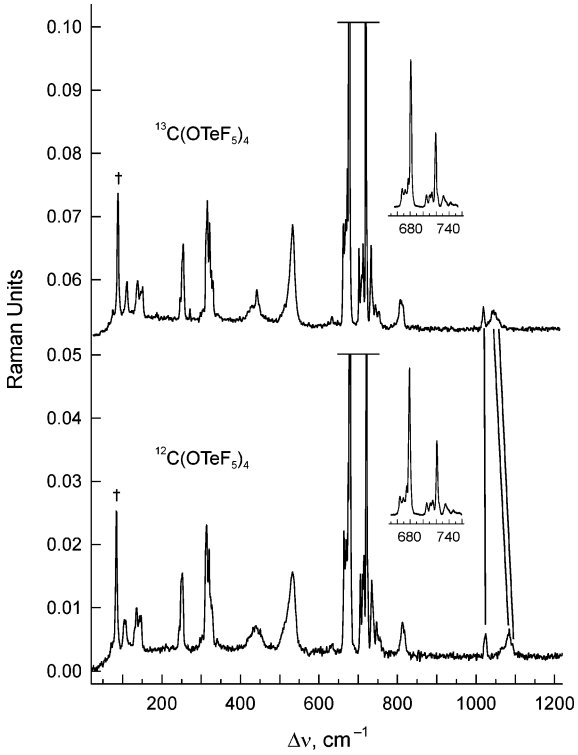

Figure 3. Raman spectra of natural abundance and ^{13}C-enriched (99%) $C(OTeF_5)_4$ recorded at −160 °C using 1064-nm excitation. Lines indicate bands that shift upon $^{12/13}$C substitution. Inset intensities must be multiplied by four. The dagger (†) denotes an instrumental artifact.

$C(OTeF_5)_4$, the O−C−O angles do not differ from the ideal tetrahedral angle by more than $\pm 3\sigma$, with averages of 113(2)° for two angles and 108(2)° for four angles. On the basis of O−E−O angle considerations alone, both $E(OTeF_5)_4^{-/0}$ species have local symmetries that are closer to S_4 than to D_{2d} symmetry. Taking into account intramolecular O···O contact distances as per the LCP approach,[33] the $B(OTeF_5)_4^-$ anion and $C(OTeF_5)_4$ have two *aa* (2.465(8) and 2.31(3) Å) and four *ac* (2.371(5) and 2.23(3) Å) contacts, respectively, which are indicative of local S_4 symmetry for both species. A comparative study and fuller discussion of the symmetries of $E(OTeF_5)_4^{-/0}$ are provided in Computational Results, where the experimental structures are also shown to possess S_4 symmetry based on their experimental and calculated Te−O−E−O torsion angles (Table 2).

Raman Spectra of $C(OTeF_5)_4$ and $B(OTeF_5)_4^-$. The low-temperature Raman spectra of natural abundance and ^{13}C-enriched $C(OTeF_5)_4$ and that of $[N(CH_3)_4][B(OTeF_5)_4]$ are shown in Figures 3 and 4, respectively. The experimental and calculated frequencies are summarized in Tables 3 and S2 for $C(OTeF_5)_4$ and $B(OTeF_5)_4^-$, respectively. The vibrational modes of $C(OTeF_5)_4$ and $B(OTeF_5)_4^-$ were assigned under S_4 symmetry and belong to the irreducible representation $\Gamma = 20A + 21B + 20E$, with all 81 modes Raman active and the B and E modes infrared active. The low-temperature, solid-state Raman spectra of $^{12/13}C(OTeF_5)_4$ and $B(OTeF_5)_4^-$ displayed bands that agree with and could be readily assigned to their $OTeF_5$ groups by comparison with the calculated frequencies and the published frequencies of other $OTeF_5$ derivatives,[22−25] therefore requiring no further comment.

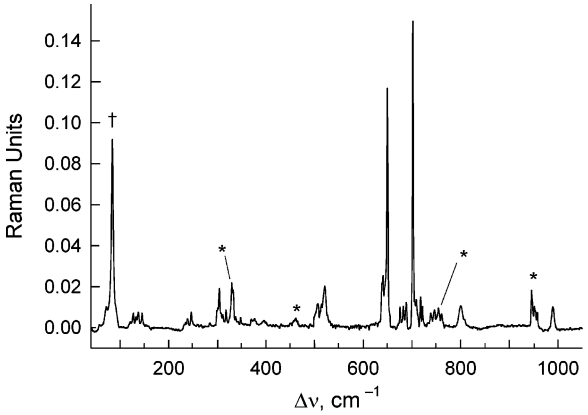

Figure 4. Raman spectrum of $[N(CH_3)_4][B(OTeF_5)_4]$ recorded at −160 °C using 1064-nm excitation. Asterisks (∗) denote $N(CH_3)_4^+$ cation bands and the dagger (†) denotes an instrumental artifact.

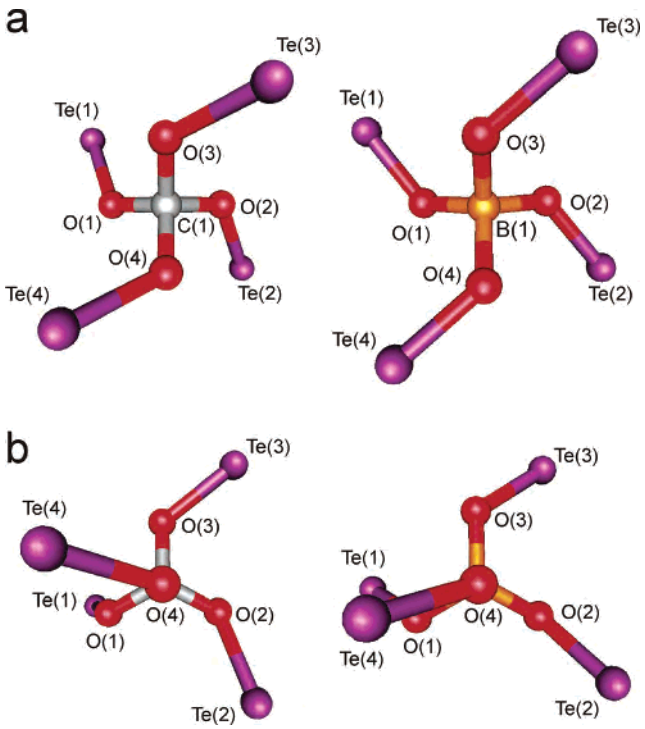

Figure 5. Calculated local geometries (S_4 symmetry) for the $E(OTe)_4$ moieties of $E(OTeF_5)_4^{0/-}$ (E = C, B) species (a) looking down the collinear S_4- and C_2-axes and (b) looking along the E(1)−O(4) bond.

Bands associated with the CO_4 moiety were assigned in the natural abundance spectrum of $C(OTeF_5)_4$ to 1078.5, 1084.0 cm^{-1} (E, ν(CO−CO); 1063.5, 1070.5 cm^{-1} (B, $\nu(CO_2-CO_2)$); 1023.2 cm^{-1} (A, $\nu(CO_4-4TeO)$), which are in good agreement with their respective calculated frequencies (SVWN: 1096.6, 1082.7, and 1010.0 cm^{-1}). Upon ^{13}C isotopic enrichment, the ν(CO−CO) and $\nu(CO_2-CO_2)$ bands exhibited isotopic shifts to lower frequency of 29.5, 31.1 cm^{-1} (calcd, 29.7 cm^{-1}) and 25.6, 24.8 cm^{-1} (calcd, 28.9 cm^{-1}), respectively. In contrast, $\nu(CO_4-4TeO)$ shifted by only 1.6 cm^{-1} (calcd, 1.0 cm^{-1}), which is consistent with the near-zero displacement of the carbon atom in the latter mode. The vibrational frequencies of $C(OTeF_5)_4$ are higher than those of $B(OTeF_5)_4^-$; the B−O stretching frequencies occur at 989 cm^{-1}, which is broad (E, ν(BO−BO) and B, $\nu(BO_2-BO_2)$) and at 951, 958 cm^{-1} (A, $\nu(BO_4-4TeO)$). The

Table 3. Experimental and Calculated Vibrational Frequencies[a] for $^{12/13}C(OTeF_5)_4$

$^{12}C(OTeF_5)_4$		$^{13}C(OTeF_5)_4$		
exptl[b]	calcd (S_4)[c]	exptl[b]	calcd (S_4)[c]	assgnts (S_4)[d]
1084.0(2) 1078.5 sh	1096.6(15)	1052.9(<1) 1049.0(<1) 1045.7(<1)	1066.1(14)	E, ν(CO – CO)
1070.5(<1) 1063.5 sh	1082.7(8)	1037.9(1) 1033.9(2)	1053.8(8)	B, $\nu(CO_2 - CO_2)$
1023.2(2)	1010.0(31)	1021.6(2)	1009.0(31)	A, $\nu(CO_4 - 4TeO)$
813.5(3)	793.6(16)	811.7(3)	792.5(16)	E, $\nu(2TeO - 2TeO)$
755.9(1)	741.1(2)	755.6(2)	739.6(1)	B, $\nu[2(TeO - TeF_a) + 2(TeF_a - TeO) + 4(TeF_{e\ trans} - TeF_{e\ trans})]_{small}$
747.3(2)	731.5(1) 731.1(1) 730.4(2)	748.7(2) 746.9 sh	730.9(1) 730.6(1) 730.3(2)	B, $\delta(CO_2 - CO_2) + \nu[(2(TeO - TeF_a) + 2(TeF_a - TeO) + 4(TeF_{e\ trans} - TeF_{e\ trans})]$ E, $\nu[4(TeF_{e\ trans} - TeF_{e\ trans})] + \delta(CO_2 - CO_2)_{small}$ A, $\nu[4(TeF_{e\ trans} - TeF_{e\ trans})]$
736.8 sh 734.7(6)	728.3(2) 725.0(6) 720.1(<1)	737.3 sh 734.7(5)	728.1(2) 724.9(6) 719.9(<1)	B, $\delta(CO_2 - CO_2)_{small} + \nu[4(TeF_{e\ trans} - TeF_{e\ trans})]$ A, $\nu[4(TeF_{e\ trans} - TeF_{e\ trans})]$ E, $\nu[2(TeF_{e\ trans} - TeF_{e\ trans}) + 2(TeF_{2e\ cis} - TeF_{2e\ cis})]$
721.0(44)	707.9(21)	718.8(50) 714.2(8)	708.0(20)	A, $\nu(4TeF_a)$
714.5(10) 710.8(6)	699.2(6)	708.9(7)	699.1(6)	E, $\nu(2TeF_a - 2TeF_a)$
705.3(9)	691.3(10)	703.5(7)	690.2(10)	B, $\delta(CO_2 - CO_2) + \nu(2TeF_a - 2TeF_a)$
678.2(100)	659.2 (91)	677.8(100)	659.2(91)	A, $\nu(4TeF_{4e})$
668.3(11) 663.8(11)	657.5 (2) 653.7(4) 651.3(5) 650.5(7) 649.6(2)	667.2(13) 663.9(12)	657.8(2) 653.7(4) 651.2(4) 650.3(7) 649.4(2)	B, $\delta(4COTe) + \nu(2TeF_{4e} - 2TeF_{4e})$ B, $\nu[4(TeF_{2e\ trans} - TeF_{2e\ trans})]$ E, $\nu[(2TeF_{2e\ trans} - 2TeF_{2e\ trans})]$ A, $\nu[4(TeF_{2e\ trans} - TeF_{2e\ trans})]$ E, $\nu[(TeF_{4e} - TeF_{4e}) + 2(TeF_{2e\ trans} - TeF_{2e\ trans})]$
632.7(<1)	640.4(3)	632.3(<1)	640.9(3)	B, $\delta(2COTe - 2COTe) + \nu(4TeF_{4e})$
533.0(11) 512.0 sh	539.9(56)	538.1(11)	543.3(56)	A, $\delta(4COTe)$
442.1(2)	444.3(5)	441.5(1)	446.1(5)	A, $\rho_t(4COTe)$
428.4(3)	429.7(2)	428.2(4) 422.0 sh	429.1(2)	E, $\rho_w(CO_2)$
338.7(<1)	360.9(<1)		361.0(<1)	B, $\rho_w(CO_4)$
324.3(9)	325.8(<1)	329.6 sh 325.4(6)	327.1(<1)	A, $\rho_r(CO_2 - CO_2) + \delta(2TeF_{4e\ umbrella} - 2TeF_{4e\ umbrella})$
319.6(14) 313.3(16) 302. 3(1)	306.6(1) 305.9(1) 303.4(2) 302.1(<1) 300.0(1) 299.2(1) 298.2(<1) 296.1(<1)	319.3(13) 312.6(11) 302.1(1)	307.4(1) 307.0(1) 304.0(2) 302.9(<1) 300.7(1) 299.2(1) 298.4(<1) 297.1(<1)	strongly coupled deformation and torsion modes involving both $OTeF_5$ and COTe moieties
268.7(<1)	291.5(1) 285.7(2) 284.1(<1) 281.7(1)	269.0(1)	292.8(1) 285.7(2) 284.0(<1) 282.1(<1)	
251.7(11) 248.6(11) 243.8 sh	236.3(<1) 234.1(2) 233.9(<1) 232.6(2) 230.4(<1)	251.7(7) 247.2(8)	236.5(<1) 234.7(2) 233.9(<1) 233.0(2) 231.7(<1)	

Table 3 (Continued)

$^{12}C(OTeF_5)_4$		$^{13}C(OTeF_5)_4$		
exptl[b]	calcd (S_4)[c]	exptl[b]	calcd (S_4)[c]	assgnts (S_4)[d]
184.5(<1)	200.5(<1)	185.5(<1)	202.4(<1)	strongly coupled deformations and torsion modes involving both $OTeF_5$ and COTe moieties
	194.0(<1)		196.6(<1)	
	193.4(<1)		196.1(<1)	
	189.5(<1)		191.6(<1)	
145.2(4)	133.9(1)	145.5(5)	134.3(1)	
142.3(4)	129.7(<1)	140.6(4)	131.0(<1)	
135.0(4)	127.8(1)	133.8(4)	130.5(<1)	
	123.4(<1)		124.3(1)	
	119.9(<1)		120.9(<1)	
107.6(1)	98.1(1)	107.6(5)	99.7(1)	
	93.0(<1)		97.4(<1)	
	46.6(<1)		46.9(<1)	
	38.5(<1)		38.9(<1)	
	33.2(<1)		36.9(<1)	
	32.0(<1)		32.9(<1)	
	27.1(<1)		27.0(<1)	
	22.4(<1)		25.4(<1)	
	17.0(<1)		24.7(<1)	

[a] Frequencies are given in cm^{-1}. [b] Values in parentheses denote experimental relative Raman intensities. The abbreviation denotes a shoulder (sh). [c] SVWN/(SDB-)cc-pVTZ. Raman intensities (in $Å^4$ amu^{-1}) are given in parentheses. [d] The abbreviations denote stretch (ν), bend (δ), twist (ρ_t), wag (ρ_w), and rock (ρ_r). Bond elongations and angle openings are denoted by plus (+) signs, and bond contractions and angle closings are denoted by minus (−) signs. The notations F_a and F_e refer to the axial fluorine atom and the four equatorial fluorine atoms of the $OTeF_5$ group, respectively; the notations TeF_{2e} and TeF_{4e} indicate that two and four, respectively, Te−F_e bond stretching motions are in phase. The notations $F_{e\ trans}$ and $F_{e\ cis}$ indicate that the fluorine atoms are trans and cis to each other, respectively.

$^{10/11}B$ isotopic shifts were not observed but have been calculated (Table S2). No pure O−C−O or O−B−O bending modes are predicted by computational methods; rather, they are strongly coupled to TeO and TeF stretching modes and have not been explicitly assigned in Tables 3 and S2.

Computational Results. The geometric parameters and vibrational frequencies (see Raman Spectroscopy) were calculated using DFT (SVWN) methods for both $C(OTeF_5)_4$ and $B(OTeF_5)_4^-$. All-electron correlation consistent (cc-pVTZ) basis sets were used for all atoms other than tellurium, for which a semirelativistic large core pseudopotential ((SDB-)cc-pVTZ) basis set was used. Natural bond orbital (NBO) analyses were carried out on the DFT-optimized geometries using HF methods. Total energies for experimental geometries were derived from single-point calculations.

(a) Geometries. The initial $C(OTeF_5)_4$ and $B(OTeF_5)_4^-$ geometries used in the optimization were very close to square planar about the central E atom with all E−O−Te angles close to linear and $OTeF_5$ groups pseudo-octahedral with two Te−F_e bonds and the Te−F_a bond of each $OTeF_5$ being essentially coplanar with the EO_4 moiety. The starting geometry had C_1 symmetry and the initial calculations were done at the HF/(SDB-)cc-pVTZ level of theory which gave two local minima. As indicated by the three groups of Te−O−E−O dihedral bond angles (vide infra and Figure 5), the calculated geometries were close to S_4 symmetry. Both systems were then optimized using SVWN methods at C_1 symmetry, resulting in all frequencies real for both systems. All geometrical parameters, including the Te−O−E−O torsion angles, were comparable to the experimental values. With the use of the coordinates from the latter calculations, both systems were optimized at the SVWN level at S_4 symmetry resulting in all frequencies real for $C(OTeF_5)_4$ and one imaginary frequency for $B(OTeF_5)_4^-$. While the Te−O−C−O angles were similar to those under C_1 symmetry, the Te−O−B−O angles had changed significantly. In an attempt to obtain all frequencies real for $B(OTeF_5)_4^-$ at the SVWN level, a further geometry optimization was carried out starting from the optimized S_4 (SVWN) geometry of $C(OTeF_5)_4$ and produced an energy-minimized S_4 geometry with all frequencies real and Te−O−B−O dihedral bond angles that differed from those obtained previously for S_4 (one imaginary frequency) and C_1 symmetries.

The calculated bond lengths and bond angles associated with the C_1 and S_4 energy-minimized (SVWN/(SDB-)cc-pVTZ) geometries of $C(OTeF_5)_4$ and $B(OTeF_5)_4^-$ all fall within the range of the experimentally determined values, with the exception of the calculated C−O−Te angles which were approximately 5° smaller. The calculated Te−O−C−O torsion angles for both C_1 and S_4 symmetries of $C(OTeF_5)_4$ are similar to the experimental torsion angles and are consistent with $C(OTeF_5)_4$ being well isolated in the structure

Table 4. Calculated[a] Natural Bond Orbital (NBO) Charges, Valencies, and Bond Orders for $C(OTeF_5)_4$ and $B(OTeF_5)_4^-$

	$C(OTeF_5)_4$ (S_4)		$B(OTeF_5)_4^-$ (S_4)[b]			$C(OTeF_5)_4$ (S_4)	$B(OTeF_5)_4^-$ (S_4)[b]
	charge	valency	charge	valency		bond order	bond order
E	1.199	3.264	1.046	2.684	E−O	0.910	0.658
O	−0.946	1.163	−1.000	1.225	O−Te	0.498	0.655
Te	3.965	3.039	3.547	3.237	Te−F_a	0.500	0.511
F_a	−0.660	0.471	−0.613	0.470	Te−F_e	0.487	0.508
F_e	−0.666	0.454	−0.615	0.468	Te−$F_{e'}$	0.491	0.509
$F_{e'}$	−0.662	0.453	−0.606	0.470	Te−$F_{e''}$	0.482	0.504
$F_{e''}$	−0.665	0.449	−0.610	0.469	Te−$F_{e'''}$	0.490	0.511
$F_{e'''}$	−0.666	0.459	−0.614	0.473			
$OTeF_5$ group	−0.300		−0.511				

[a] SVWN/(SDB-)cc-pVTZ//HF/(SDB-)cc-pVTZ. The symbols F_a and $F_e/F_{e'}/F_{e''}/F_{e'''}$ denote axial and equatorial fluorine atoms, respectively, where $F_e/F_{e'}/F_{e''}/F_{e'''}$ symbols are nonequivalent under S_4 symmetry. [b] The geometrical parameters correspond to the optimized S_4 geometry having the lowest energy.

(see X-ray crystal structure section). In contrast, the Te−O−B−O torsion angles of $B(OTeF_5)_4^-$ vary significantly. The C_1-structure is only slightly higher in energy than the S_4-structure, but the Te−O−B−O torsion angles are in better agreement with the experimental values. This suggests that the solid-state geometry of $B(OTeF_5)_4^-$, because of its ionic nature, is more susceptible to crystal packing effects than the carbon analogue. When the largest set of calculated Te−O−B−O torsion angles decreases, S_4 symmetry is maintained by concomitant increases in the intermediate set of angles and decreases in the smallest set of angles (Tables 2 and S1).

(b) Natural Bond Orbital (NBO) Analyses. Natural atomic charges, Mayer natural atomic orbital valencies, and natural atomic orbital bond orders between atoms in $C(OTeF_5)_4$ and $B(OTeF_5)_4^-$, calculated using HF methods, are given in Table 4.

(i) Natural Atomic Charges for $C(OTeF_5)_4$ and $B(OTeF_5)_4^-$. The NBO analyses for $C(OTeF_5)_4$ and $B(OTeF_5)_4^-$ were carried out at the HF/(SDB-)cc-pVTZ level of theory so that the results could be compared with previous calculations for $C(OTeF_5)_3^+$ and $B(OTeF_5)_3$.[20] The positive charge on the carbon atom of $C(OTeF_5)_4$ (1.20) is lower than that of $C(OTeF_5)_3^+$ (1.30), with the boron analogues exhibiting parallel behavior, i.e., $B(OTeF_5)_4^-$ (1.25) and $B(OTeF_5)_3$ (1.45). The higher boron charges relative to the carbon charges of their carbon analogues reflect the higher electronegativity of carbon. As a result of the lower electronegativity of boron and higher net negative charges of $B(OTeF_5)_3$ and $B(OTeF_5)_4^-$, the charge separations between the central atom and the ligands are greater for the boron analogues. Thus, the total charge on a $OTeF_5$ group of $B(OTeF_5)_4^-$ (−0.56) is more negative than that of $C(OTeF_5)_4$ (−0.30) with a parallel trend for $B(OTeF_5)_3$ (−0.48) and $C(OTeF_5)_3^+$ (−0.10). The charge separations are indicative of the greater polarity of the B−O bonds when compared with those of their carbon analogues.

(ii) Bond Orders and Valencies for $C(OTeF_5)_4$ and $B(OTeF_5)_4^-$. The C−O bond order for $C(OTeF_5)_4$ (0.91) is significantly higher than that of $B(OTeF_5)_4^-$ (0.62) and, again, reflects the greater polarities of the B−O bonds. The trend is also exhibited by $C(OTeF_5)_3^+$ (1.01) and $B(OTeF_5)_3$ (0.73).[20] The bond order differences in going from $E(OTeF_5)_3^{0/+}$ to $E(OTeF_5)_4^{-/0}$ are 0.11/0.10, which reflect the differences in E ← O π donation in going from trigonal planar to tetrahedral local geometries. The valencies at E are also consistent with the greater polarities of the B−O bonds in $B(OTeF_5)_4^-$ (2.68) when compared to $C(OTeF_5)_4$ (3.26), with parallel behavior exhibited by $B(OTeF_5)_3$ (2.18) and $C(OTeF_5)_3^+$ (3.04).[20]

Conclusions

The present study provides a synthetic route to $C(OTeF_5)_4$ and describes its structural characterization in solution and in the solid state. In contrast with the room-temperature stability of $C(OTeF_5)_4$ in SO_2ClF, dissolution of $C(OTeF_5)_4$ in CH_3CN results in rapid decomposition of $C(OTeF_5)_4$ at 10 °C to give CO_2 and $O(TeF_5)_2$, with the reaction likely proceeding through the reactive intermediate, $O{=}C(OTeF_5)_2$. With the availability of a more precise crystal structure for $B(OTeF_5)_4^-$, determined in the course of the present work, and that of $C(OTeF_5)_4$, it has proven possible to assess the local symmetries of $E(OTeF_5)_4^{0/-}$ by LCP predictions and by comparisons of Te−O−E−O torsion angles. Both approaches established that the geometries of $C(OTeF_5)_4$ and $B(OTeF_5)_4^-$ are best represented by S_4 rather than by C_1 or D_{2d} symmetries. Electronic structure calculations accurately reproduced the experimental geometric parameters and are in accord with assignments of the experimental symmetries to S_4. They have also aided in the vibrational assignments of $E(OTeF_5)_4^{0/-}$ and reproduced the $^{12/13}C$ isotopic shifts associated with the vibrational frequencies of the CO_4 moiety of $C(OTeF_5)_4$.

Experimental Section

Apparatus and Materials. Manipulations of volatile materials were carried out on a glass vacuum line, and nonvolatile materials were handled inside a drybox as previously described.[34] All reaction vessels were constructed from $^1/_4$-in. o.d. FEP tubing, joined to Kel-F valves by means of compression fittings, and were dried under dynamic vacuum for several hours prior to passivation with 1 atm of fluorine gas for 8−12 h. All vacuum-line connections were made by use of $^1/_4$-in. 316 stainless steel Swagelok Ultratorr unions fitted with Viton O-rings. Sulfuryl chloride fluoride, SO_2ClF (Allied Chemical), was purified by the literature method.[35] Carbon tetrabromide (BDH Chemicals, 98%) was

(34) Casteel, W. J., Jr.; Kolb, P.; LeBlond, N.; Mercier, H. P. A.; Schrobilgen, G. J. *Inorg. Chem.* **1996**, *35*, 929−942.
(35) Schrobilgen, G. J.; Holloway, J. H.; Granger, P.; Brevard, C. *Inorg. Chem.* **1978**, *17*, 980−987.

purified by sublimation at approximately 60 °C under dynamic vacuum. Carbon-13 enriched carbon tetrabromide (99 atom % ^{13}C, Aldrich) was used without further purification. The compound, BrOTeF$_5$, was prepared and purified as previously described.[36] The salt, [N(CH$_3$)$_4$][B(OTeF$_5$)$_4$], was prepared by reaction of equimolar amounts of [N(CH$_3$)$_4$][OTeF$_5$] and B(OTeF$_5$)$_3$ in CH$_2$Cl$_2$ using a procedure similar to that used for the preparation of [N(*n*-Bu)$_4$][B(OTeF$_5$)$_4$].[9]

Preparation of Natural Abundance and ^{13}C-Enriched C(OTeF$_5$)$_4$. On a glass vacuum line, BrOTeF$_5$ (0.3908 g, 1.227 mmol) was condensed into a preweighed glass vessel fitted with a 4-mm J. Young glass/Teflon stopcock at −196 °C under static vacuum. Inside the drybox, CBr$_4$ (0.1015 g, 0.3061 mmol) was added to a $^1/_4$-in. o.d. FEP reaction vessel fitted with a Kel-F valve. The reaction vessel was removed from the drybox and connected to a glass vacuum line, where SO$_2$ClF solvent (approximately 1.5 mL) was condensed onto CBr$_4$ under static vacuum at −78 °C, followed by condensation of BrOTeF$_5$ onto the sample under static vacuum at −196 °C. Warming to −78 °C under autogenous pressure resulted in a vigorous reaction which was indicated by rapid boiling of the solvent and a color change from a bright ruby red solution to a dull red-brown solution of Br$_2$ and a white precipitate. The reaction mixture was warmed to 0 °C after 1 h, at which point the white precipitate dissolved. Removal of SO$_2$ClF (−78 °C) and Br$_2$ (0 °C) under dynamic vacuum yielded colorless, microcrystalline C(OTeF$_5$)$_4$ in nearly quantitative yield. The product sublimes slowly at room temperature under static vacuum and melts at 33.6 °C as determined by DSC (vide infra). Carbon-13 enriched C(OTeF$_5$)$_4$ was prepared in a similar manner by reaction of 0.4232 g (1.3286 mmol) of BrOTeF$_5$ with 0.1104 g (0.3319 mmol) of 99% ^{13}C-enriched CBr$_4$ in SO$_2$ClF.

Raman Spectroscopy. (a) Raman Sample Preparation. Natural abundance and ^{13}C-enriched samples of C(OTeF$_5$)$_4$ and [N(CH$_3$)$_4$][B(OTeF$_5$)$_4$] were transferred by means of a solid syringe into 5-mm o.d. glass tubes fused to $^1/_4$-in. o.d. lengths of glass tubing which were, in turn, attached to 4-mm J. Young glass/Teflon stopcocks by means of $^1/_4$-in. 316 stainless steel Swagelok Ultratorr unions fitted with Viton O-rings. The tubes were vacuum-dried for 8−12 h prior to use.

(b) Raman Instrumentation and Spectral Acquisition. The low-temperature (−160 °C) Raman spectra of microcrystalline samples of natural abundance and ^{13}C-enriched C(OTeF$_5$)$_4$ and [N(CH$_3$)$_4$][B(OTeF$_5$)$_4$] were recorded on a Bruker RFS 100 FT Raman spectrometer using 1064-nm excitation and a resolution of 1 cm^{-1} as previously described.[37] The spectra were recorded using a laser power of 300 mW and a total of 1000−1500 scans.

Nuclear Magnetic Resonance Spectoscopy. (a) NMR Sample Preparation. Samples of natural abundance and ^{13}C-enriched C(OTeF$_5$)$_4$ were transferred by means of a solid syringe into 5-mm o.d. glass NMR tubes (Wilmad) fused to $^1/_4$-in. o.d. lengths of glass tubing which were, in turn, attached to 4-mm J. Young glass/Teflon stopcocks by means of $^1/_4$-in. 316 stainless steel Swagelok Ultratorr unions fitted with Viton O-rings. The tubes were vacuum-dried for 8−12 h prior to use. Sulfuryl chloride fluoride (approximately 0.75 mL) was condensed onto the sample at −196 °C on a glass vacuum line. The NMR tubes were then flame sealed under dynamic vacuum and stored at −196 °C until NMR spectra could be acquired.

(b) NMR Instrumentation and Spectral Acquisition. Nuclear magnetic resonance spectra were recorded unlocked (field drift < 1 Hz h^{-1}) on a Bruker DRX-500 spectrometer equipped with a 11.744 T cryomagnet. The ^{13}C NMR spectrum of ^{13}C-enriched C(OTeF$_5$)$_4$ was recorded unlocked (field drift < 0.1 Hz h^{-1}) on a Bruker AV-600 spectrometer equipped with a 14.095 T cryomagnet.

The ^{19}F (^{125}Te) NMR spectra were obtained at 470.592 (157.869) MHz using a 5-mm combination ^{1}H/^{19}F (broad-band inverse) probe. The spectra were recorded in 64K (128K) memories, with a spectral width setting of 24 (94) kHz, yielding a data point resolution of 0.36 (0.72) Hz/data point and acquisition times of 1.39 (0.69) s. A relaxation delay of 0.1 s was applied, and 2000 (50 000) transients were typically accumulated using a pulse width of 2.5 (5.3) μs, corresponding to a bulk magnetization tip angle, θ, of approximately 90°. A line-broadening of 0.1 (5) Hz was used in the exponential multiplication of the free induction decays prior to Fourier transformation. In the case of the ^{19}F NMR spectrum of the 99% ^{13}C-enriched C(OTeF$_5$)$_4$, the spectrum was processed using Gaussian multiplication for resolution enhancement (line broadening, −2.0 Hz; Gaussian broadening factor, 0.80 s) prior to Fourier transformation.

The ^{13}C NMR spectrum of ^{13}C-enriched C(OTeF$_5$)$_4$ was obtained at 150.903 MHz using a 5 mm triple-resonance broadband inverse ^{1}H/^{13}C probe. The spectrum was recorded in a 64K memory, with a spectral width setting of 36.2 kHz, yielding a data point resolution of 0.55 Hz/data point and acquisition times of 0.90 s. A relaxation delay of 2.0 s was applied, and 25 000 transients were accumulated using a pulse width of 13.8 μs, corresponding to a bulk magnetization tip angle, θ, of approximately 30°. A line broadening of 0.2 Hz was used in the exponential multiplication of the free induction decays prior to Fourier transformation.

The ^{13}C, ^{19}F, and ^{125}Te NMR spectra were referenced externally at 30 °C to samples of neat TMS, CFCl$_3$, and Te(CH$_3$)$_2$, respectively. The chemical shift convention used is that a positive (negative) sign denotes a chemical shift to high (low) frequency of the reference compound.

Spectral simulations were carried out using the program MEXICO[38] to accurately determine both the ^{19}F−^{19}F and the ^{13}C−^{19}F couplings in this strongly coupled spectrum.

X-ray Crystallography. (a) Crystal Growth. (i) C(OTeF$_5$)$_4$. Approximately 0.2 g of C(OTeF$_5$)$_4$ was transferred inside a drybox by means of a solid syringe into a 10-mm o.d. glass tube fused to a $^1/_4$-in. o.d. length of glass tubing which was, in turn, connected to a 4-mm J. Young glass/Teflon stopcock using a $^1/_4$-in. 316 stainless steel Swagelok Ultratorr union with Viton O-rings. The vessel was then removed from the drybox and connected to a glass vacuum line, where it was flame sealed under dynamic vacuum at −196 °C. Large, colorless crystals were grown by sublimation over a period of approximately 1 week at ambient temperatures, after which time the glass tube was returned to the drybox where it was cut open. Several crystals were selected under a microscope attached to the drybox, heat sealed inside 0.1−0.4-mm Lindemann glass capillaries, and stored at room temperature prior to mounting on the diffractometer. The crystal used in this study was a block having the dimensions 0.45 mm × 0.35 mm × 0.30 mm.

(ii) [N(CH$_3$)$_4$][B(OTeF$_5$)$_4$]. Approximately 0.2 g of compound was transferred into a T-shaped $^1/_4$-in. o.d. FEP reaction vessel. Methylene chloride was then condensed onto the salt under static vacuum at −196 °C (approximately 1.5 mL). The salt was dissolved at 50 °C, and crystals were grown by slow cooling of the solution from 50 °C to room temperature over a period of 6 h inside the vertical arm of the reaction vessel. Colorless, needle-

(36) Gerken, M.; Kolb, P.; Wegner, A.; Mercier, H. P. A.; Borrmann, H.; Dixon, D. A.; Schrobilgen, G. J. *Inorg. Chem.* **2000**, *39*, 2813−2824.
(37) Gerken, M.; Dixon, D. A.; Schrobilgen, G. J. *Inorg. Chem.* **2000**, *39*, 4244−4255.
(38) Bain, A. *MEXICO*, release 3.0; McMaster University: Hamilton, Ontario, Canada, 2002.

shaped crystals were isolated by decanting the solvent into the horizontal arm, followed by drying under dynamic vacuum at −20 °C. The crystals were mounted as previously described.[37] The $[N(CH_3)_4][B(OTeF_5)_4]$ crystal used for this study had the dimensions 0.18 mm × 0.05-mm × 0.04 mm.

(b) X-ray Data Collection. (i) $C(OTeF_5)_4$. The crystal was centered on a P4 Siemens diffractometer, equipped with a Siemens SMART 1K CCD area detector, controlled by SMART,[39] and a rotating anode emitting Kα radiation monochromated ($\lambda = 0.710\ 73$ Å) by a graphite crystal. Diffraction data collection (−30 °C) consisted of a full φ-rotation at $\chi = 0°$ using 0.3° (1040 + 30) frames, followed by a series of short (80 frames) ω scans at various φ and χ settings to fill the gaps. The crystal-to-detector distance was 4.999 cm, and the data collection was carried out in a 512 × 512 pixel mode using 2 × 2 pixel binning. Processing of the raw data was completed using SAINT+,[39] which applied Lorentz and polarization corrections to three-dimensionally integrated diffraction spots. The program SADABS[40] was used for the scaling of diffraction data, the application of a decay correction, and an empirical absorption correction based on the intensity ratios of redundant reflections.

(ii) $[N(CH_3)_4][B(OTeF_5)_4]$. The crystal was centered on a Bruker SMART APEX II diffractometer, equipped with an APEX II 4K CCD area detector and a three-axis goniometer, controlled by the APEX2 Graphical User Interface (GUI) software,[41] and a sealed tube X-ray source (Mo target) emitting Kα radiation monochromated ($\lambda = 0.710\ 73$ Å) by a graphite crystal. Diffraction data collection (−170 °C) consisted of a full φ-rotation at a fixed $\chi = 54.74°$ with 0.36° (1010) frames, followed by a series of short (250 frames) ω scans at various φ settings to fill the gaps. The crystal-to-detector distance was 4.969 cm, and the data collection was carried out in a 512 × 512 pixel mode using 2 × 2 pixel binning. Processing of the raw data was completed using the APEX2 GUI software,[41] which applied Lorentz and polarization corrections to three-dimensionally integrated diffraction spots. The program SADABS[42] was used for the scaling of diffraction data, the application of a decay correction, and an empirical absorption correction based on the intensity ratios of redundant reflections.

(c) Solutions and Refinements of the Structures. The XPREP[43,44] program was used to confirm the unit cell dimensions and the crystal lattices. The solutions were obtained by direct methods, which located the positions of the atoms defining the $C(OTeF_5)_4$ molecules and the $[N(CH_3)_4][B(OTeF_5)_4]$ structural units, except for the H-atom positions, which were calculated. The final refinement was obtained by introducing anisotropic thermal parameters and the recommended weightings for all of the atoms except hydrogen atoms. The maximum electron densities in the final difference Fourier map were located near the heavy atoms. All calculations were performed using the SHELXTL package[43,44] for the structure determination, solution refinement, and the molecular graphics. In the case of the disordered $C(OTeF_5)_4$ molecules, the geometries of the $OTeF_5$ ligands were first approximated using the geometric parameters of a nondisordered ligand. The positions of the carbon and tellurium atoms were also refined.

Differential Scanning Calorimetry. Inside the drybox, 0.008 69 g of $C(OTeF_5)_4$ was loaded into a preweighed cold-welded aluminum pan inside the drybox. The pan was closed by a pierced aluminum lid and weighed again to obtain the mass of the compound by difference. A TA Instruments DSC 2910 modulated differential scanning calorimeter was used to determine the phase transition temperatures of $C(OTeF_5)_4$. The temperature was reduced from 25 to −125 °C at a rate of −15 °C min^{-1} and then increased to 125 °C at a rate of 15 °C min^{-1}. An identical run was repeated on the same sample, where the absence of discernible transitions indicated that sample decomposition and/or reaction with the aluminum sample container had occurred.

Calculations. Electronic structure calculations were carried out using HF and DFT (SVWN) methods using the program Gaussian 03 (revision C.02).[45] The standard, all-electron cc-pVTZ basis sets, as implemented in the Gaussian program, were utilized for all elements except Te, for which the semirelativistic large core (RLC) pseudopotential basis set (SDB-)cc-pVTZ was used.[46] The program GaussView 3.07[47] was used to visualize the vibrational displacements that form the basis of the vibrational mode descriptions given in Tables 3 and S2. Natural bond orbital analyses were performed using HF densities with the NBO program (version 3.1).[48−50]

Acknowledgment. This paper is dedicated to our friend and colleague, Prof. Dr. Dieter Naumann, on the occasion of his 65th birthday and in recognition of his many outstanding contributions to the field of fluorine chemistry. We thank the donors of the Petroleum Research Fund, administered by the American Chemical Society, for support of this work under Grant ACS-PRF No. 40959-AC3. We also thank the Natural Sciences and Engineering Research Council (NSERC) of Canada for the award of a postgraduate scholarship (M.D.M.) and for support in the form of a research grant (G.J.S.).

(39) *SMART*, release 5.611, and *SAINT+*, release 6.02; Siemens Energy and Automation Inc.: Madison, WI, 1999.
(40) Sheldrick, G. M. *SADABS* (*Siemens Area Detector Absorption Corrections*), version 2.03; Siemens Analytical X-ray Instruments, Inc.: Madison, WI, 1999.
(41) *APEX2*, release 2.0-2; Bruker AXS Inc.: Madison, WI, 2005.
(42) Sheldrick, G. M. *SADABS* (*Siemens Area Detector Absorption Corrections*), version 2.10; Siemens Analytical X-ray Instruments, Inc.: Madison, WI, 2004.
(43) Sheldrick, G. M. *SHELXTL*, release 5.1; Siemens Analytical X-ray Instruments, Inc.: Madison, WI, 1998.
(44) Sheldrick, G. M. *SHELXTL*, release 6.14; Siemens Analytical X-ray Instruments, Inc.: Madison, WI, 2000−2003.
(45) Frisch, M. J.; Trucks, G. W.; Schlegel, H. B.; Scuseria, G. E.; Robb, M. A.; Cheeseman, J. R.; Montgomery, J. A. J.; Vreven, T.; Kudin, K. N.; Burant, J. C.; Millam, J. M.; Iyengar, S. S.; Tomasi, J.; Barone, V.; Mennucci, B.; Cossi, M.; Scalmani, G.; Rega, N.; Petersson, G. A.; Nakatsuji, H.; Hada, M.; Ehara, M.; Toyota, K.; Fukuda, R.; Hasegawa, J.; Ishida, M.; Nakajima, T.; Honda, Y.; Kitao, O.; Nakai, H.; Klene, M.; Li, X.; Knox, J. E.; Hratchian, H. P.; Cross, J. B.; Adamo, C.; Jaramillo, J.; Gomperts, R.; Stratmann, R. E.; Yazyev, O.; Austin, A. J.; Cammi, R.; Pomelli, C.; Ochterski, J. W.; Ayala, P. Y.; Morokuma, K.; Voth, G. A.; Salvador, P.; Dannenberg, J. J.; Zakrzewski, V. G.; Dapprich, S.; Daniels, A. D.; Strain, M. C.; Farkas, O.; Malick, D. K.; Rabuck, A. D.; Raghavachari, K.; Foresman, J. B.; Ortiz, J. V.; Cui, Q.; Baboul, A. G.; Clifford, S.; Cioslowski, J.; Stefanov, B. B.; Liu, G.; Liashenko, A.; Piskorz, P.; Komaromi, I.; Martin, R. L.; Fox, D. J.; Keith, T.; Al-Laham, M. A.; Peng, C. Y.; Nanayakkara, A.; Challacombe, M.; Gill, P. M. W.; Johnson, B.; Chen, W.; Wong, M. W.; Gonzalez, C.; Pople, J. A. Gaussian 03, revision C.02; Gaussian, Inc.: Pittsburgh, PA, 2003.
(46) Basis sets were obtained from the Extensible Computational Chemistry Environment Basis Set Database, version 2/25/04, as developed and distributed by the Molecular Science Computing Facility, Environmental and Molecular Science Laboratory, which is part of the Pacific Northwest Laboratory, P.O. Box 999, Richland, WA 99352.
(47) Dennington, R., II; Keith, T.; Milliam, J.; Eppinnnett, K.; Hovell, W.L.; Gilliland, R. *GaussView*, version 3.07; Semichem, Inc.: Shawnee Mission, KS, 2003.
(48) Reed, A. E.; Weinstock, R. B.; Weinhold, F. *J. Chem. Phys.* **1985**, *83*, 735−746.
(49) Reed, A. E.; Curtiss, L. A.; Weinhold, F. *Chem. Rev.* **1988**, *88*, 899−926.
(50) Glendening, E. D.; Reed, A. E.; Carpenter, J. E.; Weinhold, F. *NBO*, version 3.1; Gaussian, Inc.: Pittsburgh, PA, 1990.

Supporting Information Available: Two different orientations of the disordered molecules in the unit cell of $C(OTeF_5)_4$ (Figure S1), full list of Te−O−E−O torsion angles for $E(OTeF_5)_4^{-/0}$ (E = B, C) (Table S2), full list of experimental and calculated frequencies for $E(OTeF_5)_4^{-/0}$ (E = B, C) (Table S2), and X-ray crystallographic files in CIF format for the structural determinations of $C(OTeF_5)_4$ and $[N(CH_3)_4][B(OTeF_5)_4]$. This material is available free of charge via the Internet at http://pubs.acs.org.

IC700362G